Egypt. J. Chem. **Vol. 65,** No. 2 pp. 249 - 258 (2022)

Egyptian Journal of Chemistry

http://ejchem.journals.ekb.eg/

Synthesis, modification, characterization, radiolabeling and *in vivo* behavior of carboxylated nanographene oxide sheets as a tumor imaging agent

Mohammed F. Elsabagh[1,2]. Hend Fayez[1]. Mohammed A. Motaleb[1]. Wafaa A. Zaghary[3]. Tamer M. Sakr[2,4*]

[1]*Labeled Compounds Department, Hot Labs Center, Egyptian Atomic Energy Authority, Cairo 13759, Egypt.*

[2]*Radioisotopes Production Facility, Second Egyptian Research Reactor Complex, Egyptian Atomic Energy Authority, Cairo 13759, Egypt.*

[3]*Department of Pharmaceutical Chemistry, Faculty of Pharmacy, Helwan University, Cairo, Egypt.*

[4]*Radioactive Isotopes and Generator Department, Hot Labs Center, Egyptian Atomic Energy Authority, Cairo 13759, Egypt.*

Abstract

Graphene is a crystalline form of carbon that is regarded as a novel and innovative product. carboxylated nanographene oxide sheets (NGO-COOH) was synthesized using a modified Hummer's method and assess their medical significance. NGO-COOH were successfully synthesized with an average size of 40 nm. FT-IR, UV–Vis, XPS spectrophotometry, and TEM were used to thoroughly describe them. The cytotoxicity function of NGO-COOH nanosheets were tested against cell line. The radiosynthesized [^{99m}Tc]Tc-NGO-COOH had a high radiolabeling yield (97.3±0.45 %). The tumor uptake of [^{99m}Tc]Tc-NGO-COOH nanosheets in an *in vivo* biodistribution model in tumor-bearing mice was high. NGO-COOH nanosheets may be a promising imaging agent, based on these findings.

key words: Nanographene sheets, Technetium-99m, Nanosynthesis, Tumor imaging, Radiolabeling

.

1. Introduction

Cancer is one of the major deaths in the globe. Chemotherapy and radiotherapy are two traditional anticancer treatments that are frequently hindered by toxicity and a lack of specificity[1]. Some anticancer drugs bioavailability and effectiveness are impaired by their low water solubility, limited blood half-life, small therapeutic indexes, and high systemic toxicity [1-3]. Nanotechnology advancements have sparked new uses in cancer therapy and diagnosis [4].

Nanoparticles (NPs) are particles with a diameter of 100 nm or less that can readily pass-through cell membranes since their size is tiny. In terms of size and form, They can be prepared as stable, uniform and clearly defined characterized structures. For diagnosis or treatment, In highly selective biological mediums, NPs must be safe and biocompatible [4, 5]. The accumulation of NPs in the intended site is decreased because NPs are taken up by the reticuloendothelial system (RES). Many studies have been conducted with the aim of lowering RES uptake and rising particulate carrier concentrations at the target sites in the body[5]. Recent research has shown, nanoparticle size is critical factors in preventing RES uptake and achieving higher concentrations in the targeted site can be applied to study cell binding in both normal and cancer cells, as well as their tissue-targeting potential. Because of their small size, nanoparticles to easily permeate cell membrane through active and passive mechanisms, enabling them to serve as drug and contrast agent carriers [6, 7]. Tumor tissues have an entirely distinct vasculature system than normal tissue blood vessels. [8]. The vascular system that develops in tumour tissue has abnormal dynamics, with features such as, the lack of a basement membrane and hyperpermeability. [9]. Blood vessels have irregular diameters, irregular shape and blind ends. When tumour tissues' diffusion is restricted, they develop new blood vessels for waste elimination, and oxygen supply. Angiogenesis is the term for the process of neovascularization (the formation of new blood vessels) [10]. Enhanced permeability and retention (EPR) effect describes this type of cancer tissue phenomena. [8, 11-14].

Nanoparticles should ideally remain in the blood, spread in the body for a reasonable amount of time, and target the same studied (cancer) cells in order to achieve high relative activity rate and allow for long-term treatment. It should be degraded and excreted after the imaging process is completed [3, 15, 16].

*Corresponding author e-mail: moh_pharma2008@yahoo.com (Mohammed F. Elsabagh)

Receive Date: 10 July 2021, Revise Date: 31 July 2021, Accept Date: 08 August 2021

DOI: 10.21608/EJCHEM.2021.85086.4150

Graphene has recently been investigated for biomedical applications by a few research groups. It has been investigated for biological imaging due to its good biocompatibility, rapid cellular uptake, versatile chemical changes, and unique optical characteristics.[17]. All these previous characteristics are unique characteristics for graphene nanosheets against any other nanoparticles [18-20]. There are many nanoparticles are used in radiomedicine as radiocarrier for the radiosotopes used in medicine. Radiolabeled nanoparticles are used for diagnosis or therapy such as ^{99m}Tc-chitosan nanoparticles, ^{99m}Tc-bovine serum albumin nanoparticles, [^{99m}Tc]Tc-Aspergillus flavus synthesized copper oxide, all these nanoparticles are for diagnosis while Indium-111 labeled multifunctional superparamagnetic iron oxide nanoparticles is an example of radiolabeled nanoparticles for therapeutic action[21-26]

Due to its ideal half-life of around 6 hours, ^{99m}Tc is a radionuclide frequently utilized in radioactive tracers investigations as a single-photon emission computed tomography (SPECT) imaging agent[27], ensuring that the patient is not subjected to harmful radiation. [28-30]. ^{99m}Tc also is of favorable energy (140 KeV) of γ -ray yielding a high counting efficacy [31-33].

In this context, we're looking at using carboxylated nanographene sheets to carry [^{99m}Tc]Tc for imaging (e.g. for image-guided drug delivery). We introduce the preparation and characterization of carboxylated nanographene sheets made from a biocompatible and biodegradable graphene and labeling of these carboxylated nanographene oxide sheets with ^{99m}Tc. The cellular absorption and a preliminary *in vivo* evaluation of [^{99m}Tc]Tc-carboxylated nanogaraphene oxide sheets in a tumor bearing mice are also presented and discussed.

1. Experimental:

1.1. Materials

1.1.1. Chemicals

Graphite, $NaNO_3$, H_2SO_4, $KMnO_4$, H_2O_2 and NaOH were bought from Sigma (St. Louis, Mo., USA). Fetal Bovine serum, DMEM, RPMI-1640, HEPES buffer solution, L-glutamine and gentamycin were purchased from Lonza (Belgium).

1.1.2. Radioactive material

Technetium-99m was eluted as pertechnetate from ^{99}Mo/^{99m}Tc generator that was received as a gift from Radio-isotopes Production Facility (RPF), Egyptian Atomic Energy Authority (EAEA), Cairo, Egypt.

1.1.3. Mammalian cell lines:

Normal human lung fibroblast cells (MRC-5) were collected from the American Type Culture Collection (ATCC, Rockville, MD).

1.2. Synthesis of carboxylated nanographene oxide sheets (NGO-COOH)

The sheets of carboxylated nanographene oxide were synthesized. To form graphite oxide suspension from natural graphite powder, researchers used a modified Hummers' process1.0 g graphite and 1.0 g $NaNO_3$ were first added to 50 mL H_2SO_4. After that, for 10 minutes, the mix was stirred in an ice bath, 6 g $KMnO_4$ was added gradually as it warmed to room temperature. For 2 hours, in a water bath at 35 °C, the suspension was regularly stirred. The suspension that has been prepared was then mixed with 100 mL deionized (DI) water. During the diluting step, the temperature of the suspension was kept below 60 °C. Finally, 6 mL H_2O_2 (30%) diluted in 200 mL DI water was added to the suspension to soluble manganese ions to prevent the suspension from forming residual permanganate at 6000 rpm for 10 minutes. The acids and salts that remained were extracted. The supernatant solution was centrifuged several times to remove all of the acids and salts. After ultrasonicating the obtained nanographene oxide suspension for 30 minutes, a yellow-brownish graphene oxide suspension was obtained. Any remaining unexfoliated graphitic platelets were dissolved by centrifugation at 2000 rpm for 15 minutes, and the precipitates had been eliminated. For carboxylation of nanographene oxide 10 ml NaOH (12mg/ml) was added followed by sonication for 2 hours at 800 W to convert OH groups to COOH [34-39].

1.3. Characterization of NGO-COOH nanosheets

Various techniques were used to characterize them to ascertain their form, size, surface area, chemical composition, and dispersion. Transmission electron microscopy (TEM) with an acceleration voltage of 200 kV (Ted Pella, Redding, CA, USA), and dynamic light scattering (DLS) at an acceleration voltage of 200 kV (Ted Pella, Redding, CA, USA) are two approaches for characterization (DLS), The XPS peak was deconvoluted by using Gaussian components after a Shirley background subtraction. The O/C atomic ratio of the GO sheets was evaluated using peak area ratio of the XPS core levels and the sensitivity factor of each element in XPS. Raman spectroscopy was carried out at room temperature using a HR-800 Jobin-Yvon equipped with a 532 nm Nd-YAG excitation source. UV–Visible spectrophotometry using Visible recording spectrophotometer UV-160A, Shimadzu, Japan and Fourier transforms infrared spectroscopy (FT-IR), (Mattson Instruments, Inc., New Mexico, USA was used for (FT-IR) Fourier transforms infrared spectroscopy. Samples were prepared for TEM measurements by putting 5–20 µL of NGO-COOH dispersed solution on a Cu grid and then dried under an IR lamp while the sample had been diluted by

utilizing the same sample quantity of bidistilled water for DLS measurements.

1.4. Radiolabeling of NGO-COOH nanosheets

[^{99m}Tc]TcO_4^- was eluted from ^{99}Mo/^{99m}Tc generator in hepta-oxidation state since this form is not able to label any compound on direct addition, it was eluted. So just before labeling procedure, reduction of ^{99m}Tc is required for converting $^{99m}Tc^{+7}$ from the hepta state to a favourable lower oxidation state, that can complexes with the ligand to form the radiopharmaceuticals[40].

1.5. Evaluation of Cytotoxic Effects of NGO-COOH nanosheets

1.5.1. Cell line Propagation:

The cells were grown on RPMI-1640 medium supplemented with 10% inactivated fetal calf serum and 50µg/mL gentamycin. The cells were maintained at 37ºC in a humidified atmosphere with 5% CO_2 and were subcultured 2-3 times per week.

1.5.2. Cytotoxicity evaluation using viability assay

For cytotoxicity assay, the cell lines were suspended in medium at concentration $5x10^4$ cell/well in Corning® 96-well tissue culture plates, then incubated for 24 hr. nanographene oxide was then added into 96-well plates (three replicates) to achieve twelve concentrations for it. Six vehicle controls with media were run for each 96 well plate as a control. After incubating for 24 h, the numbers of viable cells were determined by the MTT test. the concentration required to cause toxic effects in 50% of intact cells is called 50% inhibitory concentration (IC_{50}) and was estimated using Graphpad Prism software (San Diego, CA. USA) from graphic plots of the dose response curve for each conc. [41, 42].

1.6. Biodistribution study of [^{99m}Tc]Tc-NGO-COOH nanosheets

The animal study was conducted in accordance with the EAEA Committee on Animal Ethics (EAEA/2020/193) which follows the criteria set upon by the European Community for the use of animals as an experiment.

1.6.1. Tumor induction in mice

To form a solid tumor, a 0.2 ml solution of Ehrlich Ascites Carcinoma was administered intramuscularly in the right thigh of female Swiss Albino mice. The animals were well-cared for until the tumors became obvious (10-15 days). The parent tumor line (Ehrlich Ascites Carcinoma) was taken from 7-day-old Swiss Albino donor females and diluted with sterile physiological saline solution to yield 12.5 x 10^6 cells/ml[43].

1.6.2. *In vivo* biological study of [^{99m}Tc]Tc-NGO-COOH nanosheets

Biodistribution studies were carried out by the percentage injected dose per gram (%ID/g) values obtained from radioactivity distribution measured *ex vivo*. At 0.5, 1, 2, 4 h p.i., mice were euthanized and blood, solid tumor, and major organs/tissues were collected and wet-weighed. In addition, separate cohorts of the solid tumor-bearing mice were intravenously injected with [^{99m}Tc]Tc-NGO-COOH nanosheets (four mice per group). Radioactivity was detected in each tissue by a gamma-counter (Perkin Elmer) and presented as %ID/g (mean_SD)[44-46].

2. Result and Discussion:

2.1. Characterization of Carboxylated Nanographene oxide sheets (NGO-COOH nanosheets)

All small sheets within a size range of 10-77 nm (**Figure 1 a**), which was corroborated by DLS data that determined the average diameters of Carboxylated Nanographene oxide sheets to be 6.5 ~ 77 nm. The carboxylated nanographene oxide sheets are morphologically studied using transmission electron microscopy (TEM) images (**Figure 1 b**). The lateral width of the carboxylated nanographene oxide sheets was reduced by sonication from several hundreds of nanometers to less than 150 nanometers, while the thickness remained unchanged at 1–2 nanometers as measured by TEM. The presence of COOH groups in the NGO was also confirmed by FTIR measurements. As shown in (**Figure 2 a**) the appearance of absorption peaks at 3437 (sharp peak) and 1638 cm^{-1}, carbonyl group stretched due to C=C of cyclic carbon in the hybrid structure of nanographene while NG-OH can be assigned as a broad band at 3471 cm^{-1} as shown in (**Figure 2 b**) [47]. (**Figure 2 c**) presents XPS peak deconvolution of C(1s) core levels of the GO sheets. In the peak deconvolution, the peak centered at 285.0 eV was attributed to the C-C and C=C bonds. The other deconvoluted peaks located at the binding energies of 286.6, 287.4, 288.3 and 289.4 eV were assigned to the C-OH, C-O-C, C=O, and O=C-OH oxygen-containing functional groups, respectively [49–51]. The O/C atomic ratio of the GO sheets was found to be 0.47. This is consistent with the oxygen content of chemically exfoliated GO sheets reported previously [52,53]. COOH groups of NGO was confirmed by UV/Vis measurement, a peak at 232nm appears due to presence of COOH group as shown in (**Figure 3**) while NGO sheets appear at 270 nm [34, 47, 48]. Carboxylation of NGO nanosheets is done to be coated with hydrophilic moiety such as carboxylic group that helps to prevent the RES mechanism by reducing *in vivo* adsorption.

(a)

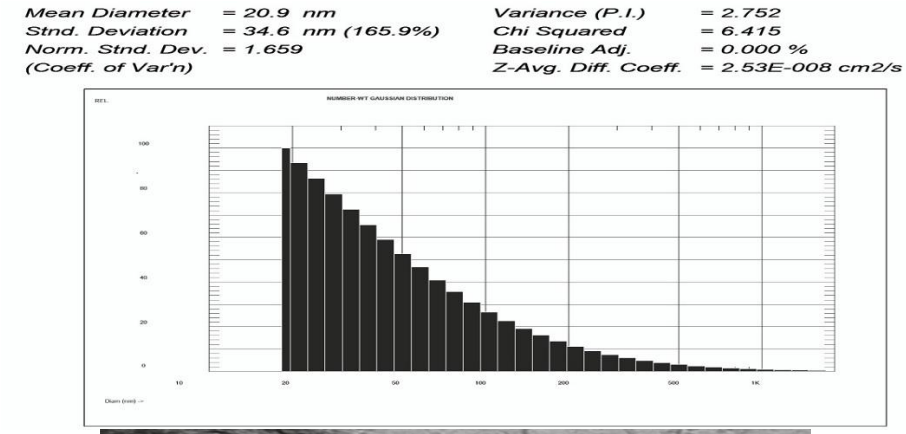

(b)

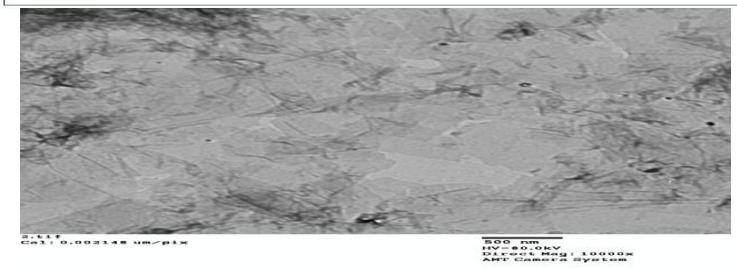

Fig. 1 Size analysis of NGO-COOH nanosheets (a) DLS scan, (b) TEM image

(a)

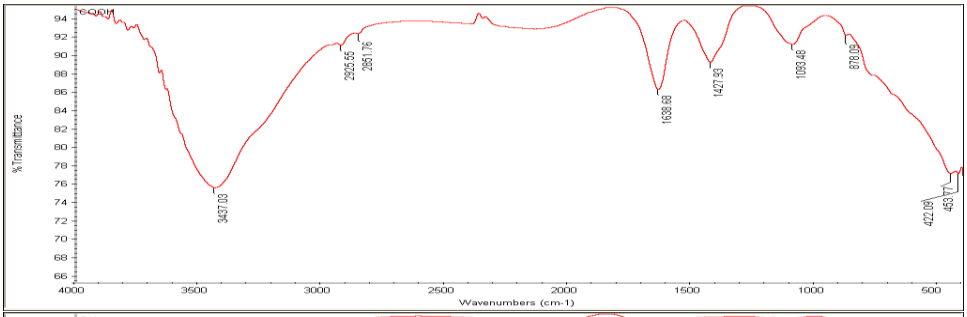

(b)

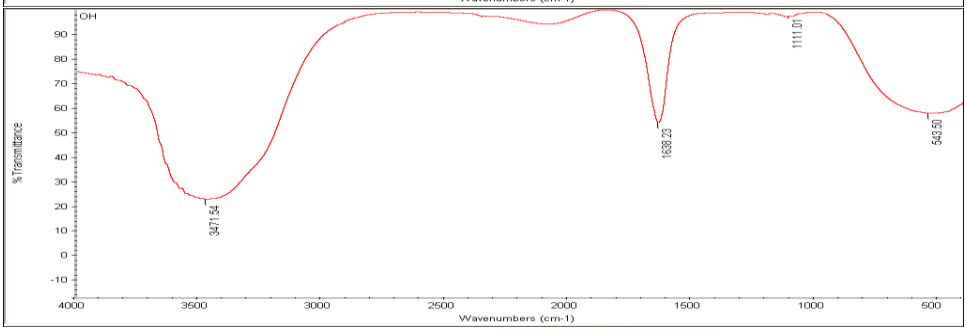

(C)

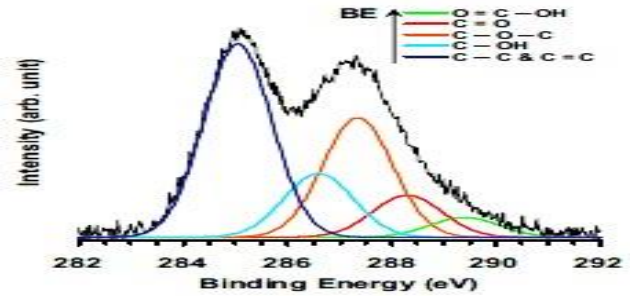

Fig. 2 The FT-IR spectra of (a) NGO-COOH nanosheets, (b) NGO-OH nanosheets and (C) XPS spectrum of NGO-COOH nanosheets

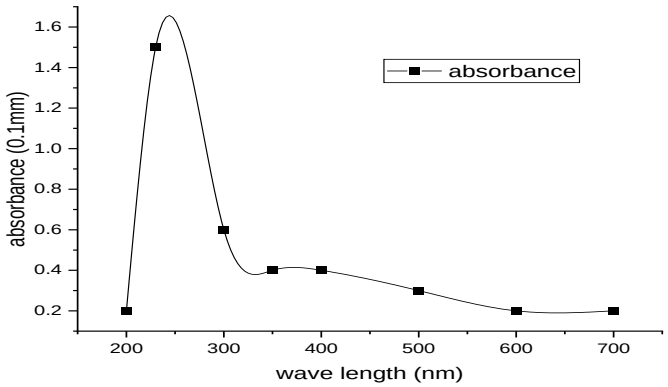

Fig. 3 UV/Vis spectra of the NGO-COOH nanosheets

2.2. Radiolabeling of NGO-COOH nanosheets

Nanosheets of [^{99m}Tc]Tc-NGO-COOH were radiolabeled as follow; 200 µl of freshly eluted [^{99m}Tc]TcO_4^- (20 MBq) was added to 15 mg sodium dithionite as reducing agent followed by adding of 500 µL carboxylated nanogaraphene oxide sheets and before measuring, the mixture was incubated for the appropriate amount of time [^{99m}Tc]Tc-carboxylated nanogaraphene oxide sheets yield. [^{99m}Tc]Tc-carboxylated nanogaraphene oxide sheets radiochemical yield was determined using (13 cm x 1 cm) strips of ascending paper chromatography and two different mobile phases were used for developing [49-53]. Acetone was used as a mobile phase to check the free [^{99m}Tc]TcO_4^-% (R_f=1) and the percent of reduced hydrolyzed [^{99m}Tc]Tc-colloid (RH-^{99m}Tc) was determined using saline as a mobile phase (R_f=0). [^{99m}Tc]Tc-NGO-COOH sheets percent was calculated as following`

$$Radiolabeled\ complex\ \% = 100-(free\_^{99m}Tc\_TcO^-_4\%+RH-^{99m}Tc\%)$$

At PH 6, 15 mg Sodium dithionite as reducing agent, 500 µl substrate amount and after 30min, We reach the optimum condition of [^{99m}Tc]Tc-carboxylated nanogaraphene oxide sheets which is 97.3% radiochemical yield as shown in (**Figure 4**)

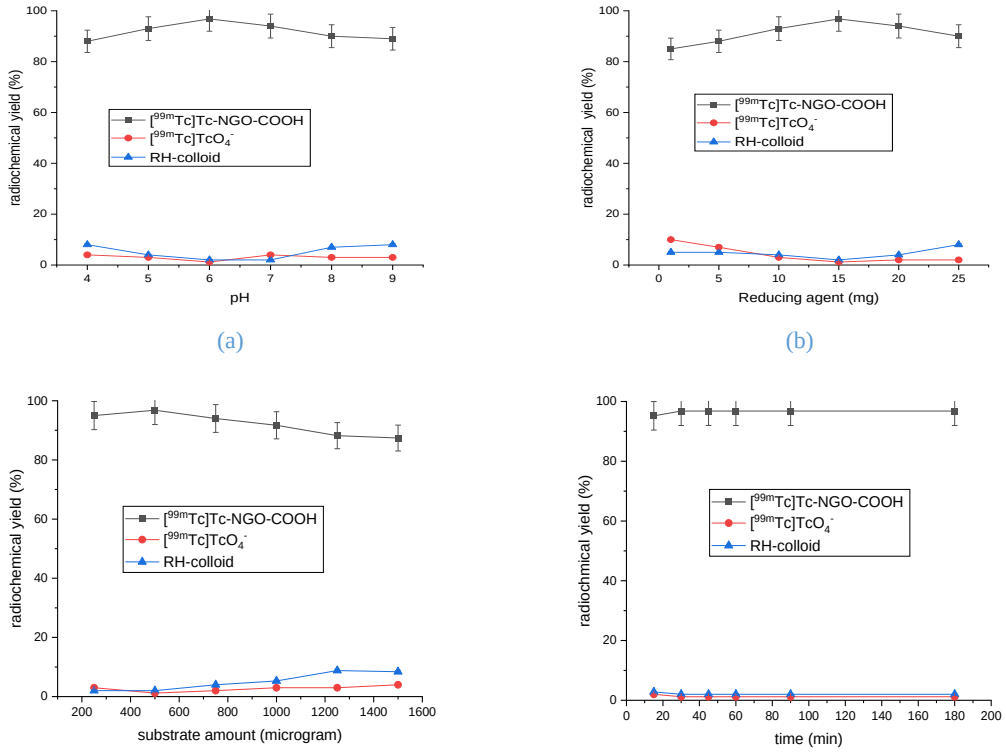

Fig. 4 Radiochemical yield of [^{99m}Tc]Tc-NGO-COOH nanosheets. **(a)** pH, **(b)** reducing agent, **(c)** substrate amount, **(d)** reaction time

2.3. In vitro stability study

[^{99m}Tc]Tc- NGO-COOH nanosheets were tested for in vitro stability of saline/serum as indicated (**Figure 5**). At 0.5, 2, 4, 6, 8 and 24 hours of post-incubating, radiochemical yields were estimated to 37 °C. The data indicated adequate radiochemical rates up to 8 hours above 97.3%. It is obvious from this work that the [^{99m}Tc]Tc- NGO-COOH nanosheets were stable enough in saline/serum, showing stability of up to 6 hours in vitro.

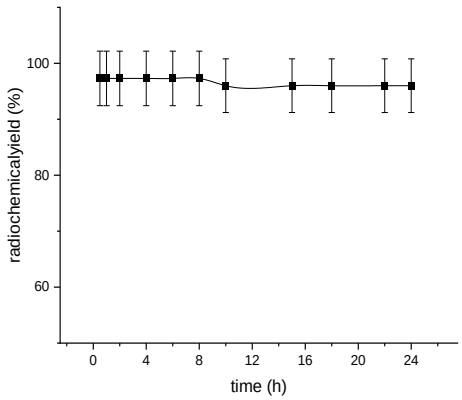

Fig. 5 [^{99m}Tc]Tc- NGO-COOH nanosheets in vitro stability in saline/serum at 37 °C followed in time

2.4. Cytotoxicity evaluation of NGO-COOH nanosheets

Inhibitory activity was detected using MTT assay under these experimental conditions with IC_{50} = 30.45 ± 0.27 µg/mL as shown in (**Figure 6**). This result illustrates the biocompatibility of NGO-COOH and how much the safety of this organic compound.

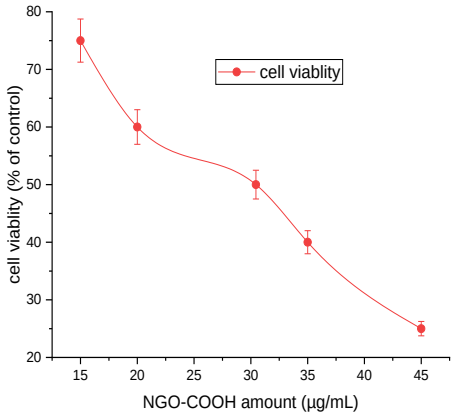

Fig. 6 Relative cell viability of NGO-COOH

2.5. Biodistribution study of NGO-COOH nanosheets

Since the hydrodynamic diameter of the NGO-COOH conjugates studied in this analysis is considerably greater than the cutoff for renal filtration (5 nm), they were cleared mainly *via* the hepatobiliary pathway[54]. [^{99m}Tc]Tc-NGO-COOH absorption in the liver was 12± 1.7, 16 ±1.2, 14.3 ±1.1, and 13 ±1.3 percent ID/g at 0.5, 1, 2, and 4 h p.i., respectively (n = 4), while blood radioactivity was 8± 1.4, 7.5±1.2, 5.5±1.1, and 5±0.4 percent ID/g at 0.5, 1, 2, and 4 h p.i., respectively. The tumor quickly acquired [^{99m}Tc]Tc- NGO-COOH (clearly apparent at 0.5 h p.i.) and the tumor uptake remained stable/time (6.5± 0.4, 7± 0.4, 9± 0.3, and 7± 0.4 %ID/g at 0.5, 1, 2, and 4 h p.i. respectively; n = 4) as shown in (**Figure 7 and Figure 8**).

Target/non-target ratio (T/NT) was used to determine the selectivity of [^{99m}Tc]Tc- NGO-COOH nanosheets for tumor sites. (**Figure 9**) showed that [^{99m}Tc]Tc-NGO-COOH nanosheets accumulated quickly in the tumour cell. The T/NT ratio for [^{99m}Tc]Tc-NGO-COOH is the ratio of tumour muscle uptake to normal muscle uptake. After 2 hours of IV injection, [^{99m}Tc]Tc-NGO-COOH nanosheets attained their peak value 9±0.5 after 2 h after IV injection. The rapid and large concentration of [^{99m}Tc]Tc- NGO-COOH nanosheets in the solid tumor suggests that it may be used as a tumor imaging agent. The high absorption of [^{99m}Tc]TcO_4^- in the stomach (14.2 ±0.35 an hour after injection) was seen in the biodistribution of the radioisotope (**Figure 10**).

NGO-COOH nanosheets with [^{99m}Tc]Tc didn't show a high stomach, suggesting no *in vivo* radiolysis, so [^{99m}Tc]Tc indicating no *in vivo* radiolysis [55]. Since more than half of the nanosheets have size larger than 25 nm, significant tumor aggregation and accumulation were reached, which may be due to the enhanced permeability and retention (EPR) effect [6, 56-59], Since tumor tissues lack a drainage lymphatic system, EPR is encouraged. Nanosheets being coated with hydrophilic moiety such as carboxylic group help to prevent the RES mechanism by reducing *in vivo* adsorption [25, 60, 61]. The stabilization of nanosheets with a hydrophilic groups are the most efficient methods for reduction of RES uptake [36, 62-65]. Since a hydrated water membrane offers strong steric hindrance, phagocytes are unable to invade remained stable during its *in vivo* studies [55, 66-68].The advantage of our prepared radiolabeled nano-system ([^{99m}Tc]Tc- NGO-COOH) is the high target/nontarget ratio which was 9 after two hours after administration while recently published radiolabeled nanosystems were with maximum T/NT ratio 3.7±0.45-7±0.5[24, 69, 70]. It is good to mention here that NGO T/NT ratio was 2±0.5 as reported[71].

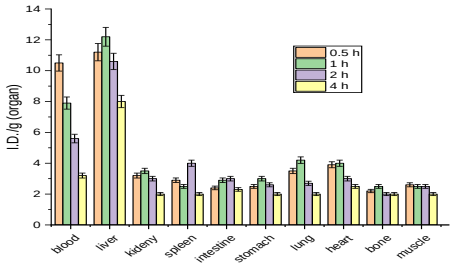

Fig. 7 *In vivo* biodistribution of [^{99m}Tc]Tc-NGO-COOH nanosheets in normal Albino mice at different time intervals post intravenous injection; I.V. (% ID/g)

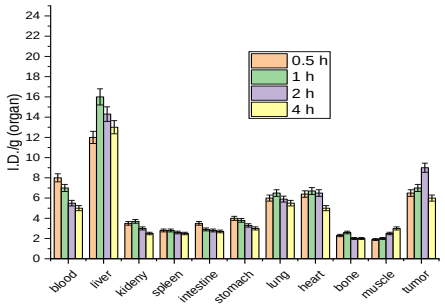

Fig. 8 *In vivo* biodistribution of [^{99m}Tc]Tc-NGO-COOH nanosheets in solid tumor-bearing Albino mice at different time intervals post intravenous injection; I.V. (% ID/g)

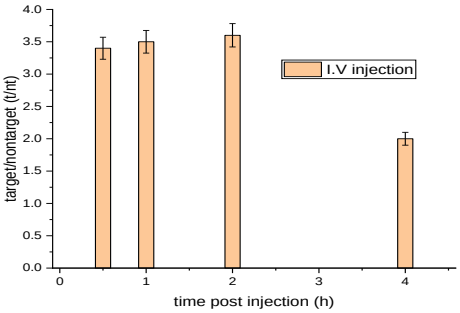

Fig. 9 T/NT ratio of [^{99m}Tc]Tc-NGO-COOH nanosheets at different times post I.V. Injection in solid tumor- tumor bearing Albino mice

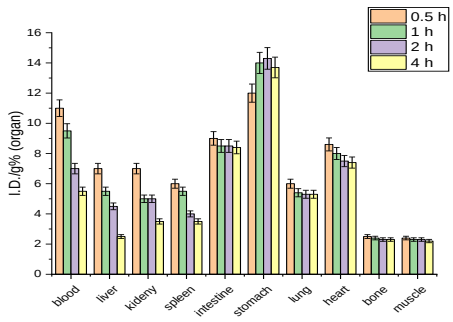

Fig. 10 *In vivo* biodistribution of [^{99m}Tc]TcO_4^-

3. Conclusion:

NGO-COOH nanosheets as a modified derivative of Nanographene oxide (NGO) sheets, has large surface area and capacity to carry a large payload so it is a novel nano-wall material that tracks to tumors *in vivo*. NGO-COOH holds promise as a versatile scaffold material for the development of molecular imaging probes. This study illustrates the feasibility of using functionalized nanographene oxide sheets for ^{99m}Tc labeling, which may have clinical effects in terms of improved tumor imaging.

4. Acknowledgement:

Prof. Tamer M. Sakr expresses his grateful appreciation and thanks for International Atomic Energy Authority (IAEA) for international collaboration and funding this work under CRP No. F22064.

Prof. Wafaa A. Zaghary expresses his grateful appreciation and thanks for Research support center, Helwan University, Egypt for funding this work.

5. Compliance with ethical standards:

Conflict of interest, all authors declared no conflict of interest.

6. References:

1. Douma, K., et al., *Nanoparticles for optical molecular imaging of atherosclerosis.* Small, 2009. **5**(5): p. 544-557.
2. DeNardo, S.J., et al., *Development of tumor targeting bioprobes (111In-chimeric L6 monoclonal antibody nanoparticles) for alternating magnetic field cancer therapy.* Clinical Cancer Research, 2005. **11**(19): p. 7087s-7092s.
3. Ronquist, K.G., et al., *Energy-requiring uptake of prostasomes and PC3 cell-derived exosomes into non-malignant and malignant cells.* Journal of extracellular vesicles, 2016. **5**(1): p. 29877.
4. Ribeiro, E., et al., *Radiolabeled block copolymer micelles for image-guided drug delivery.* International journal of pharmaceutics, 2016. **515**(1-2): p. 692-701.
5. Torchilin, V.P., *Micellar nanocarriers: pharmaceutical perspectives.* Pharmaceutical research, 2007. **24**(1): p. 1-16.
6. Varela, J.A., et al., *Quantifying size-dependent interactions between fluorescently labeled polystyrene nanoparticles and mammalian cells.* Journal of nanobiotechnology, 2012. **10**(1): p. 1-6.
7. Muthu, M.S., et al., *Theranostic vitamin E TPGS micelles of transferrin conjugation for targeted co-delivery of docetaxel and ultra bright gold*

nanoclusters. Biomaterials, 2015. **39**: p. 234-248.
8. Sugahara, K.N., et al., *Coadministration of a tumor-penetrating peptide enhances the efficacy of cancer drugs.* science, 2010. **328**(5981): p. 1031-1035.
9. Siemann, D.W., *The unique characteristics of tumor vasculature and preclinical evidence for its selective disruption by tumor-vascular disrupting agents.* Cancer treatment reviews, 2011. **37**(1): p. 63-74.
10. Byrne, J.D., T. Betancourt, and L. Brannon-Peppas, *Active targeting schemes for nanoparticle systems in cancer therapeutics.* Advanced drug delivery reviews, 2008. **60**(15): p. 1615-1626.
11. Kalyane, D., et al., *Employment of enhanced permeability and retention effect (EPR): nanoparticle-based precision tools for targeting of therapeutic and diagnostic agent in cancer.* Materials Science and Engineering: C, 2019. **98**: p. 1252-1276.
12. Balkwill, F.R., M. Capasso, and T. Hagemann, *The tumor microenvironment at a glance*. 2012, The Company of Biologists Ltd.
13. Whiteside, T., *The tumor microenvironment and its role in promoting tumor growth.* Oncogene, 2008. **27**(45): p. 5904-5912.
14. Chen, F., et al., *New horizons in tumor microenvironment biology: challenges and opportunities.* BMC medicine, 2015. **13**(1): p. 1-14.
15. Palma, G., et al., *Antitumor activity of PEGylated biodegradable nanoparticles for sustained release of docetaxel in triple-negative breast cancer.* International journal of pharmaceutics, 2014. **473**(1-2): p. 55-63.
16. Pérez-Herrero, E. and A. Fernández-Medarde, *Advanced targeted therapies in cancer: drug nanocarriers, the future of chemotherapy.* European journal of pharmaceutics and biopharmaceutics, 2015. **93**: p. 52-79.
17. Tang, Z., et al., *Constraint of DNA on functionalized graphene improves its biostability and specificity.* Small, 2010. **6**(11): p. 1205-1209.
18. Yang, Y., et al., *Graphene based materials for biomedical applications.* Materials today, 2013. **16**(10): p. 365-373.
19. Kamil, A., et al., *Modification of hummers presses for synthesis graphene oxide nano-sheets and graphene oxide/Ag nanocomposites.* Journal of Ovonic Research, 2021. **17**(3).
20. Fazaeli, Y., et al., *In vivo SPECT imaging of tumors by 198,199 Au-labeled graphene oxide nanostructures.* Materials Science and Engineering: C, 2014. **45**: p. 196-204.
21. Zolata, H., F.A. Davani, and H. Afarideh, *Synthesis, characterization and theranostic evaluation of Indium-111 labeled multifunctional superparamagnetic iron oxide nanoparticles.* Nuclear medicine and biology, 2015. **42**(2): p. 164-170.
22. Jankovic, D., et al., *90Y-labeled tin fluoride colloid as a promising therapeutic agent: Preparation, characterization, and biological study in rats.* Journal of pharmaceutical sciences, 2012. **101**(6): p. 2194-2203.
23. Buckway, B., et al., *Gold nanorod-mediated hyperthermia enhances the efficacy of HPMA copolymer-90Y conjugates in treatment of prostate tumors.* Nuclear medicine and biology, 2014. **41**(3): p. 282-289.
24. Amin, M.A., et al., *Exploitation of Aspergillus flavus synthesized copper oxide nanoparticles as a novel medical agent.* Journal of Radioanalytical and Nuclear Chemistry, 2021. **328**(1): p. 299-313.
25. Chunfu, Z., et al., *Synthesis of polyacrylamide modified magnetic nanoparticles and radiolabeling with {sup 188} Re for magnetically targeted radiotherapy.* Journal of Magnetism and Magnetic Materials, 2005. **293**.
26. Ozgur, A., et al., *Synthesis and biological evaluation of radiolabeled photosensitizer linked bovine serum albumin nanoparticles as a tumor imaging agent.* International journal of pharmaceutics, 2012. **422**(1-2): p. 472-478.
27. Mirshojaei, S.F., et al., *Radiolabelled nanoparticles: novel classification of radiopharmaceuticals for molecular imaging of cancer.* Journal of drug targeting, 2016. **24**(2): p. 91-101.
28. Das, T., et al., *A novel [109Pd] palladium labeled porphyrin for possible use in targeted radiotherapy.* Radiochimica Acta, 2008. **96**(7): p. 427-433.
29. Motaleb, M.A. and M.Y. Nassar, *Preparation, molecular modeling and biodistribution of 99m Tc-phytochlorin complex.* Journal of Radioanalytical and Nuclear Chemistry, 2014. **299**(3): p. 1759-1766.
30. Kavali, R.R., et al., *Efficient methods for the synthesis of 5-(4-[18F] fluorophenyl)-10, 15, 20-tris (3-methoxyphenyl) porphyrin as a potential imaging agent for tumor.* Journal of Labelled Compounds and Radiopharmaceuticals: The Official Journal of the International Isotope Society, 2005. **48**(10): p. 749-758.
31. Staník, R. and I. Benkovský, *99mTc-labeling and molecular modeling of short dipeptide glycyl-l-proline.* Journal of Radioanalytical and Nuclear Chemistry, 2011. **287**(3): p. 949-953.

32. Tsiapa, I., et al., *99mTc-labeled aminosilane-coated iron oxide nanoparticles for molecular imaging of αvβ3-mediated tumor expression and feasibility for hyperthermia treatment.* Journal of colloid and interface science, 2014. **433**: p. 163-175.
33. Zhu, X.-M., et al., *Enhanced cellular uptake of aminosilane-coated superparamagnetic iron oxide nanoparticles in mammalian cell lines.* International journal of nanomedicine, 2012. **7**: p. 953.
34. Zhang, L., et al., *Functional graphene oxide as a nanocarrier for controlled loading and targeted delivery of mixed anticancer drugs.* small, 2010. **6**(4): p. 537-544.
35. Rana, S. and S.B. Jonnalagadda, *Covalently functionalized nano-graphene oxide for fine chemical synthesis*, in *Functionalized Nanomaterials*. 2016, IntechOpen.
36. Hong, H., et al., *In vivo targeting and positron emission tomography imaging of tumor vasculature with 66Ga-labeled nano-graphene.* Biomaterials, 2012. **33**(16): p. 4147-4156.
37. Cornelissen, B., et al., *Nanographene oxide-based radioimmunoconstructs for in vivo targeting and SPECT imaging of HER2-positive tumors.* Biomaterials, 2013. **34**(4): p. 1146-1154.
38. Kahn, M. and W. Waldhauser, *Raman spectroscopy of carbon based films–spectra interpretation and selected applications.* BHM Berg-Und Hüttenmännische Monatshefte, 2010. **155**(11): p. 534-540.
39. Yu, Q., et al., *Graphene segregated on Ni surfaces and transferred to insulators.* Applied Physics Letters, 2008. **93**(11): p. 113103.
40. Banerjee, T., et al., *Labeling efficiency and biodistribution of Technetium-99m labeled nanoparticles: interference by colloidal tin oxide particles.* International journal of pharmaceutics, 2005. **289**(1-2): p. 189-195.
41. Mosmann, T., *Rapid colorimetric assay for cellular growth and survival: application to proliferation and cytotoxicity assays.* Journal of immunological methods, 1983. **65**(1-2): p. 55-63.
42. Gomha, S.M., S.M. Riyadh, and E.A. Mahmmoud, *Synthesis and anticancer activities of thiazoles, 1, 3-thiazines, and thiazolidine using chitosan-grafted-poly (vinylpyridine) as basic catalyst.* Heterocycles: an international journal for reviews and communications in heterocyclic chemistry, 2015. **91**(6): p. 1227-1243.
43. van der Laken, C.J., et al., *Radiolabeled interleukin-8: specific scintigraphic detection of infection within a few hours.* Journal of Nuclear Medicine, 2000. **41**(3): p. 463-469.
44. Xing, R., et al., *Hollow iron oxide nanoparticles as multidrug resistant drug delivery and imaging vehicles.* Nano research, 2013. **6**(1): p. 1-9.
45. Gundogdu, E., et al., *Radiolabeling efficiency and cell incorporation of chitosan nanoparticles.* Journal of Drug Delivery Science and Technology, 2015. **29**: p. 84-89.
46. Pascual, L., et al., *Mesoporous silica as multiple nanoparticles systems for inflammation imaging as nano-radiopharmaceuticals.* Microporous and Mesoporous Materials, 2017. **239**: p. 426-431.
47. Si, Y. and E.T. Samulski, *Synthesis of water soluble graphene.* Nano letters, 2008. **8**(6): p. 1679-1682.
48. Pasricha, R., S. Gupta, and A.K. Srivastava, *A facile and novel synthesis of Ag–graphene-based nanocomposites.* Small, 2009. **5**(20): p. 2253-2259.
49. Varacallo, M. and S. Mair, *StatPearls [Internet] StatPearls Publishing*. Treasure Island (FL): Jun, 2019. **4**.
50. Papagiannopoulou, D., *Technetium-99m radiochemistry for pharmaceutical applications.* Journal of Labelled Compounds and Radiopharmaceuticals, 2017. **60**(11): p. 502-520.
51. Sakr, T., M. Motaleb, and W. Zaghary, *Synthesis, radioiodination and in vivo evaluation of ethyl 1, 4-dihydro-7-iodo-4-oxoquinoline-3-carboxylate as a potential pulmonary perfusion scintigraphic radiopharmaceutical.* Journal of Radioanalytical and Nuclear Chemistry, 2015. **303**(1): p. 399-406.
52. Polyák, A., et al., *99mTc-labelled nanosystem as tumour imaging agent for SPECT and SPECT/CT modalities.* International journal of pharmaceutics, 2013. **449**(1-2): p. 10-17.
53. Ekinci, M., et al., *Methotrexate loaded chitosan nanoparticles: preparation, radiolabeling and in vitro evaluation for breast cancer diagnosis.* Journal of Drug Delivery Science and Technology, 2015. **30**: p. 107-113.
54. Choi, H.S., et al., *Renal clearance of quantum dots.* Nature biotechnology, 2007. **25**(10): p. 1165-1170.
55. Essa, B.M., et al., *99mTc-citrate-gold nanoparticles as a tumor tracer: synthesis, characterization, radiolabeling and in-vivo studies.* Radiochimica Acta, 2020. **108**(10): p. 809-819.
56. Swidan, M.M., et al., *Iron oxide nanoparticulate system as a cornerstone in the effective delivery of Tc-99 m radionuclide: a potential molecular imaging probe for tumor diagnosis.* DARU Journal of Pharmaceutical Sciences, 2019. **27**(1): p. 49-58.
57. Dallas, N.A., et al., *Endoglin (CD105): a marker of tumor vasculature and potential target for*

therapy. Clinical Cancer Research, 2008. **14**(7): p. 1931-1937.
58. Bitounis, D., et al., *Prospects and challenges of graphene in biomedical applications.* Advanced Materials, 2013. **25**(16): p. 2258-2268.
59. Fazaeli, Y., et al., *Grafting of [64Cu]-TPPF20 porphyrin complex on Functionalized nano-porous MCM-41 silica as a potential cancer imaging agent.* Applied Radiation and Isotopes, 2016. **112**: p. 13-19.
60. Haidar, Z.S., R.C. Hamdy, and M. Tabrizian, *Protein release kinetics for core–shell hybrid nanoparticles based on the layer-by-layer assembly of alginate and chitosan on liposomes.* Biomaterials, 2008. **29**(9): p. 1207-1215.
61. Peer, D., et al., *Systemic leukocyte-directed siRNA delivery revealing cyclin D1 as an anti-inflammatory target.* Science, 2008. **319**(5863): p. 627-630.
62. Li, S.-D. and L. Huang, *Nanoparticles evading the reticuloendothelial system: role of the supported bilayer.* Biochimica et Biophysica Acta (BBA)-Biomembranes, 2009. **1788**(10): p. 2259-2266.
63. El-Ghareb, W.I., et al., *99mTc-Doxorubicin-loaded gallic acid-gold nanoparticles (99mTc-DOX-loaded GA-Au NPs) as a multifunctional theranostic agent.* International journal of pharmaceutics, 2020. **586**: p. 119514.
64. Wang, Y., et al., *Self-assembled nanoparticles of methotrexate conjugated O-carboxymethyl chitosan: Preparation, characterization and drug release behavior in vitro.* Carbohydrate polymers, 2011. **86**(4): p. 1665-1670.
65. Assadi, M., et al., *Nanotechnology and nuclear medicine; research and preclinical applications.* Hellenic journal of nuclear medicine, 2011. **14**(2): p. 149-159.
66. Del Vecchio, S., et al., *Nuclear imaging in cancer theranostics.* The Quarterly Journal of Nuclear Medicine and Molecular Imaging, 2007. **51**(2): p. 152-63.
67. Blanco, E., et al., *Multifunctional micellar nanomedicine for cancer therapy.* Experimental biology and medicine, 2009. **234**(2): p. 123-131.
68. Singh, R., et al., *Tissue biodistribution and blood clearance rates of intravenously administered carbon nanotube radiotracers.* Proceedings of the National Academy of Sciences, 2006. **103**(9): p. 3357-3362.
69. Yang, X., et al., *cRGD-functionalized, DOX-conjugated, and 64Cu-labeled superparamagnetic iron oxide nanoparticles for targeted anticancer drug delivery and PET/MR imaging.* Biomaterials, 2011. **32**(17): p. 4151-4160.
70. Tsoukalas, C., et al., *A novel metal-based imaging probe for targeted dual-modality SPECT/MR imaging of angiogenesis.* Frontiers in chemistry, 2018. **6**: p. 224.
71. Pei, X., et al., *PEGylated nano-graphene oxide as a nanocarrier for delivering mixed anticancer drugs to improve anticancer activity.* Scientific reports, 2020. **10**(1): p. 1-15.